Heterogeneous formation and light absorption of secondary organic aerosols from acetone photochemical reactions: Remarkably enhancing effects of seeds and ammonia

Si Zhang[1], Yining Gao[1], Xinbei Xu[1], Luyao Chen[1], Can Wu[1,2], Zheng Li[1], Rongjie Li[1], Binyu Xiao[1], Xiaodi Liu[1], Rui Li[1,2], Fan Zhang[1,2], Gehui Wang[1,2]*

[1]Key Lab of Geographic Information Science of the Ministry of Education, School of Geographic Sciences, East China Normal University, Shanghai 200241, China

[2]Institute of Eco-Chongming, 20 Cuiniao Rd., Chongming, Shanghai 202150, China

*Corresponding author: Prof. Gehui Wang, Email: ghwang@geo.ecnu.edu.cn

Tel: 86-21-54341193, Fax: 86-21-54341122

Abstract: Secondary organic aerosols (SOA) from highly volatile organic compounds (VOCs) are currently not well represented in numerical models as their heterogeneous formation mechanisms in the atmosphere remain unclear. Based on the smog chamber experiments, here we investigated the yield and formation pathway of SOA from acetone photochemical reactions under low NOx condition in the presence of preexisting haze particles ($(NH_4)_2SO_4$, and NH_4HSO_4) and saline mineral particles (Na_2SO_4) under ammonia-rich conditions. Our results showed that the yield of acetone-derived SOA is remarkably enhanced via multiphase reactions in the presence of these preexisting seeds especially for the saline mineral particles. We found that aerosol acidity is a key factor controlling the formation pathways of acetone-derived SOA, in which organic acids, alcohol and carbonyls produced from acetone photochemical reactions dissolve into the aqueous phase of the preexisting seeds and subsequently esterify and/or oligomerize into SOA that consist of larger molecules on the acidic aerosols but smaller molecules on the neutral mineral aerosols. Moreover, light absorption ability of the acetone-derived SOA formed on $(NH_4)_2SO_4$ aerosols is stronger than that formed on Na_2SO_4 mineral particles especially in the presence of ammonia due to a formation of N-containing organics. By comparing with that from methylglyoxal (MGly), we found that the total SOA from acetone in the chamber is 2.8–8.2 times that from the irreversible uptake of MGly, suggesting that only considering MGly as the precursor of acetone-derived SOA will probably underestimate the role of acetone in the global SOA production since acetone abundantly exists in the troposphere.

Keywords: Volatile organic compounds; Photochemical oxidation; Aqueous-phase reaction; Polymerization; Aerosol acidity.

1. Introduction

Secondary organic aerosols (SOA) are the major component of fine particles in the atmosphere and produced from the photochemical oxidation of volatile organic compounds (VOCs) (Zhang et al., 2015a; Srivastava et al., 2022; Wang et al., 2016b), which significantly affects human health and global climate change (Jo et al., 2023; Chowdhury et al., 2022). However, current numeric models cannot predict the evolution of atmospheric SOA accurately; one of reasons is that models often only consider the partitioning process of condensable oxidation products of VOCs as the major formation pathway of SOA and neglect the contribution of heterogeneous reactions of highly volatile VOCs to atmospheric SOA (Heald et al., 2005; Li et al., 2023).

A number of researchers have reported that SOA formation can be promoted significantly in the presence of hydrated seeds by heterogeneous reactions (Wong et al., 2015; Nguyen et al., 2014; Liu et al., 2018; Ge et al., 2017). For instance, Wong et al. (2015) reported that more isoprene SOA was formed on deliquescent ammonium sulfate seeds in comparison with that on the efflorescent ones. Such an enhancing effect of multiphase chemistry on SOA formation has also be found by Liu et al. (2018) and Wang et al. (2022) in their laboratory experiments. Their results showed that SOA multiphase formation is affected by the aerosol liquid phase properties such as acidity, ionic strength and mixing state, which can alter the gas-to-particle phase partitioning of VOC and change the formation process of SOA (Zhang et al., 2023; Riva et al., 2019; Riva et al., 2016; Bateman et al., 2014; Kampf et al., 2013; Wei et al., 2022). Amorim et al. (2020) analyzed the OH reactivities of organic acids in aqueous phases with different pH, and found that all the organic acids exhibited larger OH reactivities under basic conditions than those under acidic conditions, indicating that aerosol acidity can influence the gas-particle partitioning and the multigeneration oxidation of volatile organics in liquid phase (Wei et al., 2022; Amorim et al., 2021; Amorim et al., 2020; Zhao et al., 2006; Lv et al., 2022). Moreover, a few studies reported that the uptake of VOC oxidation products by inorganic aerosols can be affected by a salting-in/salting-out effect (Waxman et al., 2015; Wang et al., 2016a). These results suggest that heterogeneous reactions of VOCs are important sources of atmospheric SOA,

which are complex and affected by many factors. Currently, only a limited number of

volatile organics, such as glyoxal, methylglyoxal (MGly), formaldehyde and epoxydiols,

have been investigated by chemical transport models for their contribution to the

atmospheric SOA through heterogeneous reactions (Heald et al., 2005; Li et al., 2023; Fu et

al., 2008; Moch et al., 2020). While the role of heterogeneous reactions in SOA formation

from many other more volatile organics in the atmosphere is still unclear and is ignored

generally by model work.

Compared to glyoxal, MGly and formaldehyde, acetone is much more volatile, which is

of a Henry's law constant (K_H) being 2–4 orders of magnitude lower than the three species

and abundantly exists in the atmosphere from the ground surface to the upper troposphere

(Seinfeld and Pandis, 2006). Acetone can be directly emitted from the natural and

anthropogenic sources and indirectly produced from oxidation of hydrocarbons (Jacob et al.,

2002; Wang et al., 2023). Photolysis and OH oxidation are main sinks of acetone in the

atmosphere, with photolysis contributing 45% of the sink, OH oxidation 30%, ocean uptake

and dry deposition to land 25% (Jacob et al., 2002). Numerous studies have reported the

reaction mechanisms of acetone's photolysis and OH oxidation, and have estimated their

contributions to hydroxyl radicals in the upper troposphere and lower stratosphere,

respectively (Stefan and Bolton, 1999; Arnold et al., 2004; Raff et al., 2005; Wang et al.,

2020). However, the role of acetone in SOA heterogeneous formation remains unclear. A

laboratory experiment showed that deliquesced inorganic aerosols may promote SOA

formation from the photochemical oxidation of acetone significantly (Ge et al., 2017), but

up to now the yield of SOA derived from acetone photochemical reactions and the impact of

inorganic aerosol physicochemical properties on SOA formation from acetone have not been

reported. Therefore, the formation mechanism and the importance of acetone-derived SOA

in the atmosphere remain unclear, where acetone ubiquitously co-exists with NH_3 and

preexisting aerosols. MGly is an important product of acetone photochemical reactions with

14% molar yield as calculated by GEOS-Chem, which can partition into aqueous phase

followed by oligomerization, oxidation by OH or/and reaction with NH_3 or organic amine to

form SOA (De Haan et al., 2019; Aiona et al., 2017; Li et al., 2021b; Yasmeen et al., 2010;

Zhang et al., 2022). Currently, the SOA module in chemical transport models primarily encompasses the homogeneous reactions of various volatility VOCs and heterogeneous reactions of isoprene epoxydiol, glyoxal, methylglyoxal, hydroxymethyl-methyl-a-lactone, 2-methylglyceric acid, and 2-methyltetrols on the aerosol surface. Notably, these models do not account for SOA formation from the heterogeneous photochemical reactions of acetone on aerosols (Fu et al., 2008; Huang et al., 2024a; Huang et al., 2024b; He et al., 2024; Zheng et al., 2023). However, Ge et al. found that other products derived from acetone photo-oxidation such as alcohols and organic acids also can dissolve into the aqueous phase and transform into SOA by esterification (Ge et al., 2017), indicating that only considering the uptake of MGly will probably underestimate the contribution of acetone to the global SOA production. Thus, it is necessary to investigate the SOA formation from acetone and compare it with MGly-SOA.

In this work, we quantitatively investigated the effects of deliquescent seeds and NH_3 on SOA formation from the photochemical reaction of acetone via chamber experiments, and compared the difference of SOA formation processes in the presence of different seed particles. We for the first time revealed a key role of seed acidity in controlling the yield and formation pathways of SOA from acetone photochemical reactions, in which NH_3 and dust particles can greatly enhance the production and light absorption of acetone-derived SOA.

2. Experiments section

2.1 Materials and methods

All batch mode experiments in this study were performed in a 4 m^3 sealed Teflon smog chamber (Figure S1). Firstly, zero air and seed particles were introduced into the chamber. Then, acetone, H_2O_2 and NH_3 were introduced sequentially for the heterogeneous reactions. The experiment details are reported by our previous studies (Ge et al., 2019; Zhang et al., 2021; Liu et al., 2021a).

Briefly, zero air produced by the Zero Air Supply (Model 111 and Model 1150, Thermo Scientific, USA) was used as the background gas in this study. Saturated water vapor flow produced by bubbling zero air through ultrapure water (Milli Q, 18.2 MΩ, Millipore Ltd., USA) was introduced into the chamber for adjusting the relative humidity (85±1.0% RH).

130   Three types of water-solutions containing Na_2SO_4, $(NH_4)_2SO_4$ and NH_4HSO_4 were nebulized

131   to produce seed particles. A polydisperse mode of wetted inorganic aerosols was generated

132   from the solutions by using a single jet atomizer (7388SJA, TSI) and directly introduced into

133   the chamber as droplets without any dessication. Reactant gases including acetone, H_2O_2,

134   NH_3 and SO_2 were added separately into the chamber along with a N_2 flow using a glass

135   syringe (Liu et al., 2022; Liu et al., 2021b).

136   **2.2 Smog chamber experiments and characterization**

137   **2.2.1. Smog chamber experiments**

138   In this study, the chamber experiments can be divided into two phases: Phase I, SOA

139   formation from the photochemical oxidation and photolysis of acetone on aerosols was

140   investigated, in which the OH radicals were produced from the photolysis of H_2O_2 under 254

141   nm UV irradiating conditions; Phase II, the effect of NH_3 on SOA formation was explored

142   under dark conditions. The H_2O_2 concentrations injected into the chamber were 2.95×10^{13}

143   molecules cm^{-3} in all experiments. The influence of different inorganic particles on the two

144   phases were studied. To compare the influence of different inorganic particles on the SOA

145   formation, SO_2 was added into the chamber after Phase II to produce $(NH_4)_2SO_4$ aerosols

146   during the Na_2SO_4 seed experiments. All the experiments were conducted under $85\pm1.0\%$ RH

147   conditions and thus all the seeds in the chamber were deliquescent. At the end of each

148   experiment, aerosol in the chamber were collected on 47 mm quartz filters and stored at

149     $-20\ °C$ prior to analysis. The experimental conditions are shown in Table S1.

150   **2.2.2. On-line monitoring**

151   RH and temperature inside the chamber were monitored online. The temperature in the

152   chamber was stabilized at $25\pm1°C$ by using air conditioners. Concentrations of VOCs and

153   SO_2 in the chamber were monitored by a proton transfer reaction time-of-flight mass

154   spectrometer (PTR-TOF-MS, Ionicon Analytik, Innsbruck, Austria) and a SO_2 analyzer

155   (Model 43i, Thermos scientific), respectively. Size distribution and mass concentration of

156   aerosols during the reaction process were measured by a scanning mobility particle sizer

157   (SMPS, model 3082, USA). The real-time chemical composition evolution of aerosols in the

158   chamber was measured by a high-resolution time-of-flight aerosol mass spectrometer (HR-

ToF-AMS, Aerodyne Research Ltd, USA), which was operated on a high sensitivity V-mode with a 30 s time resolution. Prior to the experiments, ionization efficiency of the AMS was calibrated by using 300 nm NH_4NO_3 particles and the value was 5.01×10^{-8}, and the relative ionization efficiency (RIE) for ammonium was 4.6. The RIE for sulfate was calibrated using $(NH_4)_2SO_4$ particles, and the value was 0.8.

Particle wall loss in the chamber was corrected using a total-mass-concentration-based method and the detailed descriptions were shown in Text S1 (Liu and Abbatt, 2021; Zhang et al., 2024). The wall loss of NH_3 and VOCs in the chamber was also corrected (see the details in Text S2 and S3) (Li et al., 2021a; Huang et al., 2018; Zhang et al., 2015b). Aerosol liquid water content (ALWC) was estimated using the E-AIM thermodynamic model IV, and the pH values of aerosols were calculated by Eq.1.

$$pH = -\log_{10}\left(\gamma_{H^+} m_{H^+}\right) \tag{1}$$

Where γ_{H^+} and m_{H^+} were the activity coefficient and molality of H^+ calculated by E-AIM model, respectively.

2.2.3. Off-line analysis of particles

The collected samples were extracted with 15 mL of Milli-Q pure water in an ultrasonic bath for 30 min, and filtered by a 0.45 μm PES syringe filter. The concentration of water-soluble organic carbon (WSOC) and light absorption of the extracts were analyzed by a total organic carbon analyzer (model TOC/TN-LCPH, Shimadzu Inc. Japan) and a liquid waveguide capillary cell (model LWCC3000, Ocean Insight. USA) coupled with a UV/Vis spectrophotometer (ocean insight) over a wavelength range of $200-900$ nm, respectively. Light absorption (Abs_λ) and mass absorption coefficient (MAC) of the water extracts were calculated (see the details in Text S4). In addition, the collected particles were extracted with pure methanol and analyzed for their chemical compositions using an ultrahigh-resolution orbitrap mass spectrometer (Q-Exactive Orbitrap mass spectrometer, Thermo Scientific, Germany) (Jia et al., 2023). Specifically, imidazole compounds (IMs) were determined using the orbitrap-mass spectrometry, and the detailed analysis methods were reported in our previous study (Liu et al., 2023).

2.2.4. Observation-Based Chemical Box Model

In this work, an observation-based model (OBM) incorporating the latest version 3.3.1 of MCM (MCM v3.3.1; available at http://mcm.leeds.ac.uk/MCM/) was utilized to simulate the acetone photochemical reactions in the chamber. The observation levels of acetone, acetaldehyde, formic acid and acetic acid throughout the photochemical reactions, along with meteorological parameters (temperature and relative humidity) and the initial H_2O_2 concentration, were incorporated into the OBM-MCM model as constraints. The comprehensive MCM mechanisms related to the photochemical reactions of acetone and other VOCs observed in this work were also incorporated into the OBM-MCM. The photolysis rate for H_2O_2 is 9.1×10^{-6} s^{-1}. The average concentration of OH radicals during the reactions is 5.89×10^6 molecules cm^{-3}. The time series of OH and HO_2 radical concentrations are shown in Figure S2.

3. Results and discussion

3.1. Formation of acetone-derived SOA

Figure 1 shows the time evolution of gas and particle phase species during the reaction in the presence of $(NH_4)_2SO_4$ seeds. In this study the whole smog chamber reaction process consists of two phases, of which Phase I is a photochemical reaction of acetone without $NH_3(g)$ and Phase II is a dark reaction with introduced NH_3. During the Phase I, once the light was turned on the gas phase concentrations of MGly, acetaldehyde, formic acid and acetic acid quickly increased with a decreasing acetone (Phase I, Figure 1a), while SOA were instantly produced and sharply increased to over 90 μg m^{-3} (Phase I, Figure 1b). When the concentration of SOA during the Phase I did not change and even started to decease, the light was turned off and $NH_3(g)$ was introduced into the chamber (Phase II). According to the formation time of these gas products, acetaldehyde and MGly are often taken as the first-generation products, while formic and acetic acids are usually considered as the final-generation products (Poulain et al., 2010). Oxidation state of compounds (OSc) and O/C elemental ratio of SOA in the aerosol phase continuously increased during the reaction process (Figure 1c), which is corresponding to a decreasing fraction of CHO^+ plus $C_2H_3O^+$ and an increasing fraction of CO_2^+ (Figure 1d), indicating an efficient conversion of carbonyl compounds to carboxylic acid compounds. In the Phase I, we observed an aerosol-

8

216   phase decreasing trend of molar ratio of NH_4^+ to SO_4^{2-}, which was accompanied by an

217   increasing trend of N/C ratio of SOA (Figures 1b and 1c), indicating a transformation of

218   inorganic NH_4^+ to N-containing organic compounds. Such a phenomenon can be ascribed to

219   the uptake of organic acid products and a reaction of carbonyl compounds with the

220    $(NH_4)_2SO_4$ seeds during the Phase I (Liu et al., 2023; Li et al., 2021b). The pH value of

221   particles reduced rapidly from the initial 4.89 to 1.77 after a 30 min reaction due to the

222   formation of NH_4HSO_4. The increased acidity can hinder the gas-particle partitioning of gas-

223   phase reaction products such as formic, acetic acids and methylglyoxal (Lv et al., 2022;

224   Zhao et al., 2006), as most weak acids are unable to dissociate at pH<2 (Tilgner et al., 2021).

225   Therefore, SOA formation by the partitioning process sharply decreased after the 30 min

226   reaction time, resulting a slow increase of the SOA concentration. Subsequently, the SOA is

227   primarily formed through aqueous reactions on aerosols, leading to a persistent increase in

228   the O/C, N/C ratios and oxidation state of SOA.

229   As shown in Figures 1a and 1b, after NH_3 was introduced (Phase II) the formic and

230   acetic acids decreased dramatically while SOA did not change obviously, suggesting that the

231   decreases of the gas acids were mainly resulted from the enhanced wall loss due to the

232   neutralization of NH_3 on the chamber wall. Interestingly, we found that during the dark

233   reaction OSc and O/C ratio of SOA decreased slightly but their N/C ratio increased

234   significantly by a factor of approximately two (Figure 1c), implying that chemical

235   composition of SOA changed remarkably after NH_3 was introduced, although the SOA mass

236   did not change evidently (Figure 1c, Phase II). Moreover, such a slight decrement of O/C

237   and a significant increment of N/C in the elemental compositions of SOA (Figure 1c) were

238   also accompanied by a sharp increase of CHN family fragment fractions (Figure 1d, Phase

239   II), which can be explained by a carbonyl-ammonium condensation under the dark

240   conditions that forms a C-N bond and loses a H_2O molecule (Aiona et al., 2017; Li et al.,

241   2021b; Liu et al., 2023). Such an aqueous-phase dark reaction after NH_3 was introduced can

242   be further revealed by a change in SOA composition during the Phase II, which is

243   characterized by higher fractions of $C_xH_yN_1$ fragments in the Phase II than those in the

244   Phase I (Figure 2). Organic ammonium salt would contribute NHx fragments instead of

fragments containing N, C, and O elements. Therefore, the CHN species should generated from the reactions of carbonyls with NH_3 rather than the acid-base neutralization of organic acid with NH_3 (Liu et al., 2015). As seen in Figure S3, the CHN family species mainly include CHN, CH_4N, C_2H_6N, C_2H_7N, C_2H_4N, CH_5N and C_3H_6N ions, which are similar to the fragments of N-containing organics produced from the reaction of carbonyls with $(NH_4)_2SO_4$ (De Haan et al., 2010), and increased significantly during the Phase II, resulting in an enhancing role of NH_3 on the SOA formation from acetone photochemical reaction.

3.2. Enhancing effect of seeds on the SOA formation

As shown in Figure S4, the concentration of SOA derived from acetone photochemical reactions in the presence of $(NH_4)_2SO_4$ seeds is twenty times higher than that in the absence of the seeds, suggesting that the occurrence of $(NH_4)_2SO_4$ seeds remarkably promoted the SOA formation. Such an enhancing role was also found for Na_2SO_4 and NH_4HSO_4 seeds (Figure S5). Because of the significant influence of surface area of aerosols on the multiphase reactions (Huang et al., 2016), the SOA formation amounts were normalized by the aerosol surface area (SA) to eliminate the interference of the difference in seed concentrations. As seen in Figure 3a, the normalized concentration of SOA on Na_2SO_4 seeds is two times larger than that on $(NH_4)_2SO_4$ and NH_4HSO_4 seeds, respectively, indicating that the difference in physicochemical properties of seeds are of different promoting effects on the SOA formation. MGly is one of the first-generation oxidation products of the acetone photochemical reactions and also one of the critical precursor of SOA (Li et al., 2021b). Therefore, we choose it as the target compound to explore the effect of the seeds on the SOA formation. The multiphase reactions of acetone-derived MGly in the chamber can be divided into two processes: the gas-particle partitioning and the subsequent aqueous phase reactions (Srivastava et al., 2022; Waxman et al., 2015), which are further discussed as follows:

3.2.1. The effects on the gas-to-particle phase partitioning

It has been reported that the presence of salts in aerosol aqueous phase can significantly influence the gas-particle phase partitioning of MGly, which can decrease the solubility of MGly, i.e., salting out effect (Waxman et al., 2015). In this study, the effective Henry's law constants ($K_{H, salt}$) of MGly in the aqueous phase of various seeds were further estimated by

274 Eq.2 (Waxman et al., 2015; Cui et al., 2021).

$$\log \left(\frac{K_{H,w}}{K_{H,salt}}\right) = K_S c_{salt} \tag{2}$$

275 Where $K_{H,W}$ and $K_{H, salt}$ are the Henry's law constants of MGly in pure water (3.71×10^3 M

276 atm^{-1}) (Curry et al., 2018) and in a salt solution, respectively; Ks is the salting constant or

277 Setschenow constant, which is 0.16 M^{-1} used in this work (Waxman et al., 2015), supposing

278 that the K_S values are similar in the three types of inorganic aerosols (Gen et al., 2018); c_{salt}

279 is the salt concentration in molality.

280   As shown in Figure 3b, $K_{H, salt}$ of MGly on Na_2SO_4 seeds in this study is more than two

281 times that on $(NH_4)_2SO_4$ and NH_4HSO_4 seeds, respectively, because of its lower salt

282 concentration and weaker salting out effect. The acidity of aerosol aqueous phase also can

283 affect the uptake of MGly. For instance, Zhao et al. (2006) found that the effective Henry's

284 law constant of MGly decreased with an increase of aqueous acidity in their laboratory

285 experiments. As shown in Figure 3b, the pH values of Na_2SO_4, $(NH_4)_2SO_4$ and NH_4HSO_4

286 seeds in our chamber study are 7.0, 4.9 and -0.2, respectively, indicating that the neutral

287 nature of Na_2SO_4 seeds is more favorable for the uptake of MGly compared to the two other

288 acidic seeds. The SOA formation with NH_4HSO_4 seeds is similar to that with $(NH_4)_2SO_4$

289 seeds, which is possibly caused by the promotion of residual trace NH_3 in the chamber on

290 the uptake of acidic organics (Figure 3a).

291   In addition, the higher OSc and larger fraction of $C_xH_yO_z$ signals of SOA on Na_2SO_4

292 seeds (Figure 3a and Figure S6) may also be caused by enhanced uptake of carboxylic acids

293 (e.g., formic and acetic acids) in comparison with those by other two kinds of acidic seeds

294 (Huang et al., 2016), which also resulted in the less abundant formic and acetic acids in the

295 gas phase at the end of Phase I during the Na_2SO_4 seed experiment (Figure S7).

296 **3.2.2. The effects on the aqueous reaction**

297   The aqueous formation of SOA could be affected by the phase state and acidity of

298 aerosols (Amorim et al., 2020; Amorim et al., 2021; Shen et al., 2022). Since particles in all

299 the experiments of this work are deliquesced under 85% RH conditions (Wong et al., 2015;

300 Bateman et al., 2015), the influence of phase state can be neglected. Here, we focus on the

301 impact of aerosol acidity on the SOA formation pathway by characterizing the chemical

302 composition of SOA in the chamber using ESI-Q-MS technique. The mass spectra of SOA

303 formed on different seeds are shown in Figures 3c and 3d, and the detail peak assignments

304 are presented in Table S2, respectively. As shown by Figures 3c and 3d, the main peaks of

305 SOA formed on Na_2SO_4 seeds locate in the mass range lower than m/z=200, whereas the

306 main peaks of SOA formed on $(NH_4)_2SO_4$ seeds locate in the mass range larger than

307 m/z=200, clearly showing that SOA formed on neutral aerosols are dominated smaller

308 molecules while those formed on acidic aerosols are dominated larger molecules. The

309 phenomenon can be attributed to the promotion of the acid-catalyzed reactions in the

310 formation of high-order oligomers on the acidic seeds (Jang et al., 2002; Zhang et al.,

311 2015a). On the other hand, such different formation pathways of SOA also can be explained

312 by the difference of reactive oxygen species formed in the aqueous phase of the different

313 aerosols. On neutral aerosols, organic hydroperoxides produced from the reaction of

314 peroxides radicals and HO_2 radicals decompose and generate OH radicals through the

315 cleavage of the weaker O-O bond (Wei et al., 2022). Then, the OH radicals oxidize the

316 oligomers to low molecular weight (LMW) compounds (Zhao et al., 2017). In contrast, on

317 acidic aerosols the acid-catalyzed thermal decomposition of the organic hydroperoxides

318 leads to the formation of alcohol and ketone as the end products, which does not involve

319 radical formation (Wei et al., 2022; Yaremenko et al., 2016). Then, the carbonyls in the

320 aqueous phase will undergo hydration, oligomerization and acid-catalyzed aldol

321 condensation to form high molecular weight (HMW) compounds (Zhang et al., 2015a;

322 Kenseth et al., 2023; Li et al., 2021b). Such an explanation can be supported by the higher

323 OSc of SOA formed on the neutral aerosols (Figure 3a). On the other hand, the lower SOA

324 mass formed on acidic aerosols can also in part be attributed to the different reactivity of OH

325 radical to carboxylic group; OH radical does not react with the carboxyl group (COOH)

326 rapidly through H-abstraction from an O–H bond, but OH radical is more reactive to the

327 carboxylate group (ROO^-) by abstracting an electron, which can result in a high SOA yield

328 on neutral aerosols (Amorim et al., 2021; Herrmann et al., 2015).

329 **3.3 The different effect of NH_3 on SOA formation on different seeds**

As shown in Figure 4a, when NH_3 was introduced into the reaction system (Phase II), the ratio of N/C of SOA increased significantly because of the reaction of NH_4^+/NH_3 with carbonyls on acidic $(NH_4)_2SO_4$ and NH_4HSO_4 seeds, but such an evident change was not observed in the presence of NH_3 for neutral Na_2SO_4 seeds. One of the reasons is that NH_3 dissolve more readily on acidic aerosols. The gas-to-particle phase partition coefficients of NH_3 ($\varepsilon(NH_4^+)$) on different seeds were calculated (Text S5) (Guo et al., 2017; Lv et al., 2023). As shown in Figure 4b, $\varepsilon(NH_4^+)$ is zero and 1.0 for Na_2SO_4 and NH_4HSO_4 seeds, respectively, suggesting that NH_3 was almost not absorbed by Na_2SO_4 seeds but efficiently absorbed by NH_4HSO_4 seeds. The phenomenon can be confirmed by the Figure S8, more N mass partitioned on more acidic aerosols. Liu et al. (2015) analyzed the uptake of NH_3 onto SOA and also found that the uptake coefficient positively correlated with particle acidity. Several studies put forward that the reaction of NH_3 with carbonyl are likely acid-catalyzed (Zhang et al., 2015a; Liu et al., 2015). However, such a conclusion was inconsistent with the phenomenon observed by Yang et al. (2024); they found that the light absorption ability of brown carbon produced form the aqueous reactions of α-dicarbonyls with ammonium or amine increased exponentially with the increase of pH. To resolve such a disagreement. We analyzed the chemical composition of SOA detected by HR-ToF-AMS at different reaction phases. As shown in Figure S6a-d, no change was observed on Na_2SO_4 particles at Phase II after NH_3 was introduced, but the fraction of the CHN family species increased dramatically on $(NH_4)_2SO_4$ and NH_4HSO_4 particles at phase II. Hence, we supposed that NH_3 can promote the formation of N-containing SOA on acidic aerosols significantly via reacting with carbonyl compounds. To verify such an assumption, we performed additional experiments by introducing 500 ppb SO_2 into the chamber in the presence of Na_2SO_4 seeds after Phase II (Phase III, Figure S9). The addition of SO_2 resulted in $(NH_4)_2SO_4$ produced immediately in the chamber (Phase III, Figure S9a), and then the fraction of CHN species increased sharply (Phase III, Figure S9b). Such results again demonstrate the pivotal role of acidic particles in the formation of N-containing SOA.

The optical properties of the acetone-derived SOA on different particles were measured by LWCC. Compared with the light absorption spectra of SOA formed on Na_2SO_4 seeds in

the absence of SO_2, an enhanced MAC peak at ~270 nm was observed for SOA formed on $(NH_4)_2SO_4$ seeds and on Na_2SO_4 seeds with SO_2, respectively (Figure 4c). Such enhanced absorptions are in agreement with that of the products from MGly and $(NH_4)_2SO_4$ reaction, which displays prominent peaks at <240 and ~270 nm with a tail extending to >350 nm (Kasthuriarachchi et al., 2020). The increased absorption peak at 270 nm can be ascribed to a formation of imidazoles through the reaction of MGly with NH_4^+ (You et al., 2020). In this work, 1H-imidazole-4-carboxylic acid was observed for the SOA formed on $(NH_4)_2SO_4$ seeds (Figure 4d). However, the absorption peak at ~270 nm for the products of the Na_2SO_4 particles in the absence of SO_2 was weaker than that with $(NH_4)_2SO_4$ seeds significantly (Figure 4c), further confirming the enhancement effect of acidic particles on the formation of light-absorbing SOA, which is often termed as brown carbon.

3.4. Formation mechanisms of acetone-derived SOA on different seeds

Figure 5 shows the mass yield and MAC of acetone-derived SOA at the end of Phase II. Clearly, SOA is formed more readily on neutral Na_2SO_4 seeds than on acidic $(NH_4)_2SO_4$ seeds. However, in the presence of NH_3, SOA formed on $(NH_4)_2SO_4$ seeds are more light-absorbing than those formed on Na_2SO_4 aerosols, suggesting that a stronger acidity of aerosol phase is favorable for the formation of light-absorbing organics, because NH_3 cannot be taken up by neutral aerosols and thus carbonyl-ammonium condensation is only active under acidic conditions and produce light-absorbing N-containing organics.

By combining the gas and aerosol phase chemistry evolution in the chamber, chemical mechanism for SOA formation from acetone multiphase photochemical reactions on different aerosols in the presence of NH_3 was proposed (Figure 6). The photochemical reactions of acetone in this work include photolysis and oxidation by OH radicals. According to the results of OBM-MCM, the reaction rates of photolysis and OH oxidation are 3.66×10^6 and 1.32×10^7 molecules cm^{-3} s^{-1}, respectively. These two photochemical reactions produce various peroxy radical (RO_2) and undergo two RO_2 fates, RO_2+HO_2 and RO_2+RO_2 reactions. The concentrations of three main RO_2 concentrations and loss rates of two RO_2 pathways during the experiments are shown in Figure S11 and S12, respectively. Initially, CH_3O_2 and CH_3CO_3 are predominantly formed from the photolysis of acetone, and

388    $CH_3COCH_2O_2$ is generated from oxidation by OH radicals (Ge et al., 2017). Meantime, both

389   CH_3O_2 and CH_3CO_2 can be produced within the $CH_3COCH_2O_2$ chemistry, resulting in their

390   higher concentrations compared to $CH_3COCH_2O_2$ and a consistent increase in concentrations

391   throughout the experiments. Obviously, RO_2+HO_2 was the main pathway in RO_2 chemistry,

392   the loss rate of which was 3.19 times that of RO_2+RO_2 pathway. Concentrations of main

393   gaseous products from RO_2 chemistry are shown in Table S3. $C_2H_4O_3$ and $C_3H_6O_3$ are

394   intermediate volatility organic compounds (IVOCs) and can undergo gas-particle

395   partitioning readily to form SOA. Moreover, there are abundant gas-phase intermediate

396   products containing hydrophilic functional groups such as alcohol, ketone and organic acids

397   formed from acetone photochemical reactions, which can dissolve into aqueous phase and

398   undergo further oxidation reaction, esterification reaction and radical-radical reaction to

399   form SOA on particles (Poulain et al., 2010; Ge et al., 2017). For example, the dissolved

400   MGly can be hydrolyzed and then oxidized into organic acids such as pyruvic and oxalic

401   acids or proceeds to a series of oligomerizations to produce many oligomers, giving rise to

402   SOA formation. The acetone alcohol can react with acetic acid to form esters $C_5H_8O_3$ in

403   aqueous phase. The organic hydroperoxide $C_3H_6O_3$ produced from acetone-RO_2+HO_2

404   pathway also can react with acetic acid and pyruvic acid to form $C_5H_8O_4$ and $C_6H_8O_5$ in

405   particle phase, respectively. These esterification reactions can also contribute to SOA

406   formation effectively.

407   In the presence of NH_4^+, carbonyl compounds in the aerosol phase can react with free

408   NH_3 molecules and produce N-containing SOA including imine, imidazole and other

409   oligomers (Liu et al., 2023). LMW SOA are formed readily in neutral aerosol phase, while

410   HMW SOA and N-containing brown carbon are formed favorably in acidic aerosol phase,

411   because the acidic condition is favorable for the uptake of NH_3. The carbenium cations,

412   which are produced from protonation and dehydration of the hydration products of MGly

413   under acidic conditions, are the key intermediates for formation and propagation of

414   oligomerization (Ji et al., 2020). The oligomers and N-heterocycles are produced from the

415   nucleophilic addition of the negative hydroxyl O-atom of hydration products and the

416   negative N-atom of NH_3 to the carbenium cations, respectively (Li et al., 2021b; Li et al.,

417   2021a).

3.5. Comparison of SOA from acetone with that from MGly in the chamber

Currently, estimations of acetone-derived SOA by models only consider its product MGly as the precursor (Fu et al., 2008). The uptake coefficient (γ) of MGly used in their work is 2.9×10^{-3} without taking into account the influence of salting effects. Curry et al. (2018) revised the γ to 10^{-10}-10^{-6} after considering salting effects, aerosol thermodynamics, mass transfer, and irreversible reactions of organic species with OH in aqueous phase. In addition, previous laboratory studies showed a large difference among the uptake coefficients of MGly, ranging from 4.0×10^{-7} to 2.4×10^{-2} (Li et al., 2023; Li et al., 2021b). Salting effects and other VOCs such as formaldehyde and acetaldehyde also can influence the SOA formation from aqueous reaction of MGly (Rodriguez et al., 2017; Waxman et al., 2015). These documented values suggest a big uncertainty for SOA model work on MGly. Currently, the uptake coefficient (γ) of MGly is set as 2.6×10^{-4} in CMAQ v5.3 (Chen et al., 2021). Hence, the concentration of SOA formed in the chamber only from the irreversible uptake of MGly can be calculated by Eq.3 (Chen et al., 2021; Li et al., 2023).

$$\frac{\partial aqSOA}{\partial t} = \left(\frac{a}{D_g} + \frac{4}{v_{MGLY}\gamma_{MGLY}}\right)^{-1} A[MGLY] \qquad (3)$$

Where $\frac{\partial aqSOA}{\partial t}$ is the formation rate of SOA in experiments; α is the effective radius of aerosols; D_g is the gas-phase molecular diffusion coefficient; V_{MGly} is the gas-phase mean molecular speed of MGly; A is the aerosol surface area per unit air volume; [MGly] is the vapor-wall loss corrected concentration of MGly (see the details in Text S3).

As shown in Table 1, the concentrations of the total SOA-derived from acetone photochemical reaction in the chamber is 2.8-8.2 times that only from the irreversible uptake of MGly, suggesting that only considering the role of MGly will inevitably underestimate the contribution of acetone to SOA production in continental atmosphere, which is often characteristic of high loadings of acetone and aerosols.

4. Conclusions

In this study we investigated the mass yield and formation mechanism of SOA from

acetone photochemical reaction in the presence of preexisting haze particles ($(NH_4)_2SO_4$ and

NH_4HSO_4) and saline mineral particles (Na_2SO_4) under ammonia-rich conditions. We found

that the presence of seeds can significantly promote the formation of acetone-derived SOA,

and the SOA yield on Na_2SO_4 seeds is larger than that on acidic $(NH_4)_2SO_4$ and NH_4HSO_4

seeds, indicating that the differences in physicochemical properties of pre-existing aerosols

are of different promoting effects on the acetone-derived SOA formation. In comparison

with those of $(NH_4)_2SO_4$, and NH_4HSO_4 seeds, the weaker salting-out effect and lower

acidity of Na_2SO_4 seeds are in favor of the gas-to-particle partitioning of the SOA

precursors. Moreover, SOA formed on the neutral seeds are dominated by smaller molecules

with a higher OSc, while those formed on the acidic seeds are dominated by larger

molecules with a lower OSc.

Because NH_3 cannot be taken up by neutral aerosols, heterogeneous reaction of

carbonyl with ammonium is only active under acidic conditions, which produces light-

absorbing N-containing compounds such as imidazoles, resulting in the acetone-derived

SOA formed on $(NH_4)_2SO_4$ seeds more light absorbing than those formed on Na_2SO_4 seeds.

In the chamber the total SOA-derived from acetone photochemical reaction is 2.8-8.2 times

that only from the irreversible uptake of MGly, suggesting that only considering the

irreversible uptake of MGly will inevitably underestimate the contribution of acetone

photochemical reactions to SOA in the atmosphere.

References:

Aiona, P. K., Lee, H. J., Leslie, R., Lin, P., Laskin, A., Laskin, J., and Nizkorodov, S. A.: Photochemistry of products of the aqueous reaction of methylglyoxal with ammonium sulfate, ACS Earth Space Chem., 1, 522-532, 10.1021/acsearthspacechem.7b00075, 2017.

Amorim, J. V., Guo, X., Gautam, T., Fang, R., Fotang, C., Williams, F. J., and Zhao, R.: Photo-oxidation of pinic acid in the aqueous phase: a mechanistic investigation under acidic and basic pH conditions, Environ. Sci. Atmos., 1, 276-287, 10.1039/d1ea00031d, 2021.

Amorim, J. V., Wu, S., Klimchuk, K., Lau, C., Williams, F. J., Huang, Y., and Zhao, R.: pH dependence of the OH reactivity of organic acids in the aqueous phase, Environ. Sci. Technol., 54, 12484-12492, 10.1021/acs.est.0c03331, 2020.

Arnold, S. R., Chipperfield, M. P., Blitz, M. A., Heard, D. E., and Pilling, M. J.: Photodissociation of acetone: Atmospheric implications of temperature-dependent quantum yields, Geophysical Research Letters, 31, 10.1029/2003gl019099, 2004.

Bateman, A. P., Bertram, A. K., and Martin, S. T.: Hygroscopic influence on the semisolid-to-liquid transition of secondary organic materials, J. Phys. Chem. A, 119, 4386-4395, 10.1021/jp508521c, 2014.

Bateman, A. P., Gong, Z., Liu, P., Sato, B., Cirino, G., Zhang, Y., Artaxo, P., Bertram, A. K., Manzi, A. O., Rizzo, L. V., Souza, R. A. F., Zaveri, R. A., and Martin, S. T.: Sub-micrometre particulate matter is primarily in liquid form over Amazon rainforest, Nature Geosci. , 9, 34-37, 10.1038/ngeo2599, 2015.

Chen, X. Y., Zhang, Y., Zhao, J., Liu, Y. M., Shen, C., Wu, L. Q., Wang, X. M., Fan, Q., Zhou, S. Z., and Hang, J.: Regional modeling of secondary organic aerosol formation over eastern China: The impact of uptake coefficients of dicarbonyls and semivolatile process of primary organic aerosol, Sci. Total Environ., 793, 148176, 10.1016/j.scitotenv.2021.148176, 2021.

Chowdhury, S., Pozzer, A., Haines, A., Klingmüller, K., Münzel, T., Paasonen, P., Sharma, A., Venkataraman, C., and Lelieveld, J.: Global health burden of ambient $PM_{2.5}$ and the contribution of anthropogenic black carbon and organic aerosols, Environ. Int., 159, 107020, 10.1016/j.envint.2021.107020, 2022.

Cui, J. n., Sun, M., Wang, L., Guo, J., Xie, G., Zhang, J., and Zhang, R.: Gas-particle partitioning of carbonyls and its influencing factors in the urban atmosphere of Zhengzhou, China, Sci. Total Environ., 751, 142027, 10.1016/j.scitotenv.2020.142027, 2021.

Curry, L. A., Tsui, W. G., and McNeill, V. F.: Technical note: Updated parameterization of the reactive uptake of glyoxal and methylglyoxal by atmospheric aerosols and cloud droplets, Atmos. Chem. Phys., 18, 9823-9830, 10.5194/acp-18-9823-2018, 2018.

De Haan, D. O., Hawkins, L. N., Kononenko, J. A., Turley, J. J., Corrigan, A. L., Tolbert, M. A., and Jimenez, J. L.: Formation of nitrogen-containing oligomers by methylglyoxal and amines in simulated evaporating cloud droplets, Environ. Sci. Technol., 45, 984-991, 10.1021/es102933x, 2010.

De Haan, D. O., Pajunoja, A., Hawkins, L. N., Welsh, H. G., Jimenez, N. G., De Loera, A., Zauscher, M., Andretta, A. D., Joyce, B. W., De Haan, A. C., Riva, M., Cui, T. Q., Surratt, J. D., Cazaunau, M., Formenti, P., Gratien,

510   A., Pangui, E., and Doussin, J. F.: Methylamine's Effects on Methylglyoxal-Containing Aerosol: Chemical,
511   Physical, and Optical Changes, Acs Earth and Space Chemistry, 3, 1706-1716,
512   10.1021/acsearthspacechem.9b00103, 2019.

513 Fu, T. M., Jacob, D. J., Wittrock, F., Burrows, J. P., Vrekoussis, M., and Henze, D. K.: Global budgets of
514   atmospheric glyoxal and methylglyoxal, and implications for formation of secondary organic aerosols, Journal
515   of Geophysical Research-Atmospheres, 113, D15303, 10.1029/2007jd009505, 2008.

516 Ge, S., Wang, G., Zhang, S., Li, D., Xie, Y., Wu, C., Yuan, Q., Chen, J., and Zhang, H.: Abundant NH_3 in China
517   enhances atmospheric HONO production by promoting the heterogeneous reaction of SO_2 with NO_2, Environ.
518   Sci. Technol., 53, 14339-14347, 10.1021/acs.est.9b04196, 2019.

519 Ge, S. S., Xu, Y. F., and Jia, L.: Effects of inorganic seeds on secondary organic aerosol formation from
520   photochemical oxidation of acetone in a chamber, Atmospheric Environment, 170, 205-215,
521   10.1016/j.atmosenv.2017.09.036, 2017.

522 Gen, M., Huang, D. D., and Chan, C. K.: Reactive Uptake of Glyoxal by Ammonium-Containing Salt Particles
523   as a Function of Relative Humidity, Environ. Sci. Technol., 52, 6903-6911, 10.1021/acs.est.8b00606, 2018.

524 Guo, H., Liu, J., Froyd, K. D., Roberts, J. M., Veres, P. R., Hayes, P. L., Jimenez, J. L., Nenes, A., and Weber, R.
525   J.: Fine particle pH and gas–particle phase partitioning of inorganic species in Pasadena, California, during
526   the 2010 CalNex campaign, Atmos. Chem. Phys., 17, 5703-5719, 10.5194/acp-17-5703-2017, 2017.

527 He, Y., Zhao, B., Wang, S., Valorso, R., Chang, X., Yin, D., Feng, B., Camredon, M., Aumont, B., Dearden, A.,
528   Jathar, S. H., Shrivastava, M., Jiang, Z., Cappa, C. D., Yee, L. D., Seinfeld, J. H., Hao, J., and Donahue, N.
529   M.: Formation of secondary organic aerosol from wildfire emissions enhanced by long-time ageing, Nature
530   Geoscience, 10.1038/s41561-023-01355-4, 2024.

531 Heald, C. L., Jacob, D. J., Park, R. J., Russell, L. M., Huebert, B. J., Seinfeld, J. H., Liao, H., and Weber, R. J.:
532   A large organic aerosol source in the free troposphere missing from current models, Geophys. Res. Lett., 32,
533   L18809, 10.1029/2005gl023831, 2005.

534 Herrmann, H., Schaefer, T., Tilgner, A., Styler, S. A., Weller, C., Teich, M., and Otto, T.: Tropospheric aqueous-
535   phase chemistry: Kinetics, mechanisms, and its coupling to a changing gas phase, Chem. Rev., 115, 4259-
536   4334, 10.1021/cr500447k, 2015.

537 Huang, D. D., Zhang, X., Dalleska, N. F., Lignell, H., Coggon, M. M., Chan, C. M., Flagan, R. C., Seinfeld, J.
538   H., and Chan, C. K.: A note on the effects of inorganic seed aerosol on the oxidation state of secondary organic
539   aerosol—α-Pinene ozonolysis, J. Geophys. Res.: Atmos., 121, 12476–12483, 10.1002/2016jd025999, 2016.

540 Huang, L., Wu, Z. a., Liu, H., Yarwood, G., Huang, D., Wilson, G., Chen, H., Ji, D., Tao, J., Han, Z., Wang, Y.,
541   Wang, H., Huang, C., and Li, L.: An improved framework for efficiently modeling organic aerosol (OA)
542   considering primary OA evaporation and secondary OA formation from VOCs, IVOCs, and SVOCs,
543   Environmental Science: Atmospheres, 4, 1064-1078, 10.1039/d4ea00060a, 2024a.

544 Huang, Q., Lu, H., Li, J., Ying, Q., Gao, Y., Wang, H., Guo, S., Lu, K., Qin, M., and Hu, J.: Modeling the
545   molecular composition of secondary organic aerosol under highly polluted conditions: A case study in the
546   Yangtze River Delta Region in China, Science of The Total Environment, 938,
547   10.1016/j.scitotenv.2024.173327, 2024b.

548 Huang, Y., Zhao, R., Charan, S. M., Kenseth, C. M., Zhang, X., and Seinfeld, J. H.: Unified theory of vapor–
549   wall mass transport in Teflon-walled environmental chambers, Environ. Sci. Technol., 52, 2134-2142,
550   10.1021/acs.est.7b05575, 2018.

551 Jacob, D. J., Field, B. D., Jin, E. M., Bey, I., Li, Q., Logan, J. A., Yantosca, R. M., and Singh, H. B.: Atmospheric
552   budget of acetone, J. Geophys. Res.: Atmos., 107, ACH 5-1-ACH 5-17, 10.1029/2001jd000694, 2002.

553 Jang, M., Czoschke, N. M., Lee, S., and Kamens, R. M.: Heterogeneous Atmospheric Aerosol Production by

Acid-Catalyzed Particle-Phase Reactions, Science, 298, 814-817, 10.1126/science.1075798, 2002.

Ji, Y. M., Shi, Q. J., Li, Y. X., An, T. C., Zheng, J., Peng, J. F., Gao, Y. P., Chen, J. Y., Li, G. Y., Wang, Y., Zhang, F., Zhang, A. L., Zhao, J. Y., Molina, M. J., and Zhang, R. Y.: Carbenium ion-mediated oligomerization of methylglyoxal for secondary organic aerosol formation, Proc. Natl. Acad. Sci., 117, 13294-13299, 10.1073/pnas.1912235117, 2020.

Jia, L., Xu, Y., and Duan, M.: Explosive formation of secondary organic aerosol due to aerosol-fog interactions, Sci. Total Environ., 866, 161338, 10.1016/j.scitotenv.2022.161338, 2023.

Jo, D. S., Nault, B. A., Tilmes, S., Gettelman, A., McCluskey, C. S., Hodzic, A., Henze, D. K., Nawaz, M. O., Fung, K. M., and Jimenez, J. L.: Global health and climate effects of organic aerosols from different sources, Environ. Sci. Technol., 57, 13793-13807, 10.1021/acs.est.3c02823, 2023.

Kampf, C. J., Waxman, E. M., Slowik, J. G., Dommen, J., Pfaffenberger, L., Praplan, A. P., Prévôt, A. S. H., Baltensperger, U., Hoffmann, T., and Volkamer, R.: Effective Henry's Law partitioning and the salting constant of glyoxal in aerosols containing sulfate, Environ. Sci. Technol., 47, 4236-4244, 10.1021/es400083d, 2013.

Kasthuriarachchi, N. Y., Rivellini, L. H., Chen, X., Li, Y. J., and Lee, A. K. Y.: Effect of relative humidity on secondary brown carbon formation in aqueous droplets, Environ. Sci. Technol., 54, 13207-13216, 10.1021/acs.est.0c01239, 2020.

Kenseth, C. M., Hafeman, N. J., Rezgui, S. P., Chen, J., Huang, Y., Dalleska, N. F., Kjaergaard, H. G., Stoltz, B. M., Seinfeld, J. H., and Wennberg, P. O.: Particle-phase accretion forms dimer esters in pinene secondary organic aerosol, Science, 382, 787-792, 10.1126/science.adi0857, 2023.

Li, J., Zhang, H., Li, L., Ye, F., Wang, H., Guo, S., Zhang, N., Qin, M., and Hu, J.: Modeling secondary organic aerosols in China: State of the art and perspectives, Curr. Pollut. Rep., 9, 22-45, 10.1007/s40726-022-00246-3, 2023.

Li, Y. X., Zhao, J. Y., Wang, Y., Seinfeld, J. H., and Zhang, R. Y.: Multigeneration production of secondary organic aerosol from toluene photooxidation, Environmental Science & Technology, 55, 8592-8603, 10.1021/acs.est.1c02026, 2021a.

Li, Y. X., Ji, Y. M., Zhao, J. Y., Wang, Y., Shi, Q. J., Peng, J. F., Wang, Y. Y., Wang, C. Y., Zhang, F., Wang, Y. X., Seinfeld, J. H., and Zhang, R. Y.: Unexpected oligomerization of small alpha-dicarbonyls for secondary organic aerosol and brown carbon formation, Environmental Science & Technology, 55, 4430-4439, 10.1021/acs.est.0c08066, 2021b.

Liu, S., Wang, Y., Xu, X., and Wang, G.: Effects of NO2 and RH on secondary organic aerosol formation and light absorption from OH oxidation of o-xylene, Chemosphere, 308, 136541, 10.1016/j.chemosphere.2022.136541, 2022.

Liu, S., Huang, D., Wang, Y., Zhang, S., Liu, X., Wu, C., Du, W., and Wang, G.: Synergetic effects of NH_3 and NOx on the production and optical absorption of secondary organic aerosol formation from toluene photooxidation, Atmos. Chem. Phys., 21, 17759-17773, 10.5194/acp-21-17759-2021, 2021a.

Liu, S. J., Wang, Y. Q., Wang, G. H., Zhang, S., Li, D. P., Du, L., Wu, C., Du, W., and Ge, S. S.: Enhancing effect of NO_2 on the formation of light-absorbing secondary organic aerosols from toluene photooxidation, Sci. Total Environ., 794, 148714, 10.1016/j.scitotenv.2021.148714, 2021b.

Liu, T. and Abbatt, J. P. D.: Oxidation of sulfur dioxide by nitrogen dioxide accelerated at the interface of deliquesced aerosol particles, Nat. Chem., 13, 1173–1177, 10.1038/s41557-021-00777-0, 2021.

Liu, T., Huang, D. D., Li, Z., Liu, Q., Chan, M., and Chan, C. K.: Comparison of secondary organic aerosol formation from toluene on initially wet and dry ammonium sulfate particles at moderate relative humidity, Atmos. Chem. Phys., 18, 5677-5689, 10.5194/acp-18-5677-2018, 2018.

Liu, X., Wang, H., Wang, F., Lv, S., Wu, C., Zhao, Y., Zhang, S., Liu, S., Xu, X., Lei, Y., and Wang, G.: Secondary

598   formation of atmospheric brown carbon in China haze: Implication for an enhancing role of ammonia, Environ.

599   Sci. Technol., 57, 11163-11172, 10.1021/acs.est.3c03948, 2023.

600 Liu, Y., Liggio, J., Staebler, R., and Li, S. M.: Reactive uptake of ammonia to secondary organic aerosols: kinetics

601   of organonitrogen formation, Atmospheric Chemistry and Physics, 15, 13569-13584, 10.5194/acp-15-13569-

602   2015, 2015.

603 Lv, S., Wu, C., Wang, F., Liu, X., Zhang, S., Chen, Y., Zhang, F., Yang, Y., Wang, H., Huang, C., Fu, Q., Duan,

604   Y., and Wang, G.: Nitrate-enhanced gas-to-particle-phase partitioning of water-soluble organic compounds in

605   Chinese urban atmosphere: Implications for secondary organic aerosol formation, Environ. Sci. Technol. Lett.,

606   10, 14-20, 10.1021/acs.estlett.2c00894, 2023.

607 Lv, S., Wang, F., Wu, C., Chen, Y., Liu, S., Zhang, S., Li, D., Du, W., Zhang, F., Wang, H., Huang, C., Fu, Q.,

608   Duan, Y., and Wang, G.: Gas-to-aerosol phase partitioning of atmospheric water-soluble organic compounds

609   at a rural site in China: An enhancing effect of NH_3 on SOA formation, Environmental Science & Technology,

610   56, 3915-3924, 10.1021/acs.est.1c06855, 2022.

611 Moch, J. M., Dovrou, E., Mickley, L. J., Keutsch, F. N., Liu, Z., Wang, Y., Dombek, T. L., Kuwata, M.,

612   Budisulistiorini, S. H., Yang, L., Decesari, S., Paglione, M., Alexander, B., Shao, J., Munger, J. W., and Jacob,

613   D. J.: Global Importance of Hydroxymethanesulfonate in Ambient Particulate Matter: Implications for Air

614   Quality, Journal of Geophysical Research: Atmospheres, 125, D032706, 10.1029/2020jd032706, 2020.

615 Nguyen, T. B., Coggon, M. M., Bates, K. H., Zhang, X., Schwantes, R. H., Schilling, K. A., Loza, C. L., Flagan,

616   R. C., Wennberg, P. O., and Seinfeld, J. H.: Organic aerosol formation from the reactive uptake of isoprene

617   epoxydiols (IEPOX) onto non-acidified inorganic seeds, Atmos. Chem. Phys., 14, 3497-3510, 10.5194/acp-

618   14-3497-2014, 2014.

619 Poulain, L., Katrib, Y., Isikli, E., Liu, Y., Wortham, H., Mirabel, P., Le Calve, S., and Monod, A.: In-cloud

620   multiphase behaviour of acetone in the troposphere: Gas uptake, Henry's law equilibrium and aqueous phase

621   photooxidation, Chemosphere, 81, 312-320, 10.1016/j.chemosphere.2010.07.032, 2010.

622 Raff, J. D., Stevens, P. S., and Hites, R. A.: Relative Rate and Product Studies of the OH−Acetone Reaction, The

623   Journal of Physical Chemistry A, 109, 4728-4735, 10.1021/jp0501547, 2005.

624 Riva, M., Bell, D. M., Hansen, A.-M. K., Drozd, G. T., Zhang, Z., Gold, A., Imre, D., Surratt, J. D., Glasius, M.,

625   and Zelenyuk, A.: Effect of organic coatings, humidity and aerosol acidity on multiphase chemistry of isoprene

626   epoxydiols, Environ. Sci. Technol., 50, 5580-5588, 10.1021/acs.est.5b06050, 2016.

627 Riva, M., Chen, Y., Zhang, Y., Lei, Z., Olson, N. E., Boyer, H. C., Narayan, S., Yee, L. D., Green, H. S., Cui, T.,

628   Zhang, Z., Baumann, K., Fort, M., Edgerton, E., Budisulistiorini, S. H., Rose, C. A., Ribeiro, I. O., e Oliveira,

629   R. L., dos Santos, E. O., Machado, C. M. D., Szopa, S., Zhao, Y., Alves, E. G., de Sá, S. S., Hu, W., Knipping,

630   E. M., Shaw, S. L., Duvoisin Junior, S., de Souza, R. A. F., Palm, B. B., Jimenez, J.-L., Glasius, M., Goldstein,

631   A. H., Pye, H. O. T., Gold, A., Turpin, B. J., Vizuete, W., Martin, S. T., Thornton, J. A., Dutcher, C. S., Ault,

632   A. P., and Surratt, J. D.: Increasing isoprene epoxydiol-to-inorganic sulfate aerosol ratio results in extensive

633   conversion of inorganic sulfate to organosulfur forms: Implications for aerosol physicochemical properties,

634   Environ. Sci. Technol., 53, 8682-8694, 10.1021/acs.est.9b01019, 2019.

635 Rodriguez, A. A., de Loera, A., Powelson, M. H., Galloway, M. M., and Haan, D. O.: Formaldehyde and

636   Acetaldehyde Increase Aqueous-Phase Production of Imidazoles in Methylglyoxal/Amine Mixtures:

637   Quantifying a Secondary Organic Aerosol Formation Mechanism, Environmental Science & Technology

638   Letters, 4, 234-239, 10.1021/acs.estlett.7b00129, 2017.

639 Seinfeld, J. H. and Pandis, S. N.: ATMOSPHERIC CHEMISTRY AND PHYSICS: from air pollution to climate

640   change, John Wliey & Sons2006.

641 Shen, C., Zhang, W., Choczynski, J., Davies, J. F., and Zhang, H.: Phase state and relative humidity regulate the

heterogeneous oxidation kinetics and pathways of organic-inorganic mixed aerosols, Environ. Sci. Technol., 56, 15398-15407, 10.1021/acs.est.2c04670, 2022.

Srivastava, D., Vu, T. V., Tong, S., Shi, Z., and Harrison, R. M.: Formation of secondary organic aerosols from anthropogenic precursors in laboratory studies, npj Clim. Atmos. Sci., 5, 22, 10.1038/s41612-022-00238-6, 2022.

Stefan, M. I. and Bolton, J. R.: Reinvestigation of the acetone degradation mechanism in dilute aqueous solution by the UV/H2O2 process, Environmental Science & Technology, 33, 870-873, 10.1021/es9808548, 1999.

Tilgner, A., Schaefer, T., Alexander, B., Barth, M., Collett, J. L., Jr., Fahey, K. M., Nenes, A., Pye, H. O. T., Herrmann, H., and McNeill, V. F.: Acidity and the multiphase chemistry of atmospheric aqueous particles and clouds, Atmospheric Chemistry and Physics, 21, 10.5194/acp-21-13483-2021, 2021.

Wang, C., Lei, Y. D., and Wania, F.: Effect of sodium sulfate, ammonium chloride, ammonium nitrate, and salt mixtures on aqueous phase partitioning of organic compounds, Environ. Sci. Technol., 50, 12742-12749, 10.1021/acs.est.6b03525, 2016a.

Wang, F., Lv, S., Liu, X., Lei, Y., Wu, C., Chen, Y., Zhang, F., and Wang, G.: Investigation into the differences and relationships between gasSOA and aqSOA in winter haze pollution on Chongming Island, Shanghai, based on VOCs observation, Environ. Pollut., 316, 120684, 10.1016/j.envpol.2022.120684, 2023.

Wang, G., Zhang, R., Gomez, M. E., Yang, L., Levy Zamora, M., Hu, M., Lin, Y., Peng, J., Guo, S., Meng, J., Li, J., Cheng, C., Hu, T., Ren, Y., Wang, Y., Gao, J., Cao, J., An, Z., Zhou, W., Li, G., Wang, J., Tian, P., Marrero-Ortiz, W., Secrest, J., Du, Z., Zheng, J., Shang, D., Zeng, L., Shao, M., Wang, W., Huang, Y., Wang, Y., Zhu, Y., Li, Y., Hu, J., Pan, B., Cai, L., Cheng, Y., Ji, Y., Zhang, F., Rosenfeld, D., Liss, P. S., Duce, R. A., Kolb, C. E., and Molina, M. J.: Persistent sulfate formation from London Fog to Chinese haze, Proc. Natl. Acad. Sci., 113, 13630-13635, 10.1073/pnas.1616540113, 2016b.

Wang, S., Apel, E. C., Schwantes, R. H., Bates, K. H., Jacob, D. J., Fischer, E. V., Hornbrook, R. S., Hills, A. J., Emmons, L. K., Pan, L. L., Honomichl, S., Tilmes, S., Lamarque, J.-F., Yang, M., Marandino, C. A., Saltzman, E. S., de Bruyn, W., Kameyama, S., Tanimoto, H., Omori, Y., Hall, S. R., Ullmann, K., Ryerson, T. B., Thompson, C. R., Peischl, J., Daube, B. C., Commane, R., McKain, K., Sweeney, C., Thames, A. B., Miller, D. O., Brune, W. H., Diskin, G. S., DiGangi, J. P., and Wofsy, S. C.: Global atmospheric budget of acetone: Air-sea exchange and the contribution to hydroxyl radicals, Journal of Geophysical Research-Atmospheres, 125, 10.1029/2020jd032553, 2020.

Wang, Y., Cui, S., Fu, X., Zhang, Y., Wang, J., Fu, P., Ge, X., Li, H., and Wang, X.: Secondary organic aerosol formation from photooxidation of C_3H_6 under the presence of NH_3: Effects of seed particles, Environ. Res., 211, 113064, 10.1016/j.envres.2022.113064, 2022.

Waxman, E. M., Elm, J., Kurtén, T., Mikkelsen, K. V., Ziemann, P. J., and Volkamer, R.: Glyoxal and methylglyoxal setschenow salting constants in sulfate, nitrate, and chloride solutions: Measurements and gibbs energies, Environ. Sci. Technol., 49, 11500-11508, 10.1021/acs.est.5b02782, 2015.

Wei, J., Fang, T., and Shiraiwa, M.: Effects of acidity on reactive oxygen species formation from secondary organic aerosols, ACS Environ. Au, 2, 336-345, 10.1021/acsenvironau.2c00018, 2022.

Wong, J. P. S., Lee, A. K. Y., and Abbatt, J. P. D.: Impacts of sulfate seed acidity and water content on isoprene secondary organic aerosol formation, Environ. Sci. Technol., 49, 13215-13221, 10.1021/acs.est.5b02686, 2015.

Yang, L., Huang, R.-J., Yuan, W., Huang, D. D., and Huang, C.: pH-dependent aqueous-phase brown carbon formation: Rate constants and implications for solar absorption and atmospheric photochemistry, Environ. Sci. Technol., 58, 1236-1243, 10.1021/acs.est.3c07631, 2024.

Yaremenko, I. A., Vil', V. A., Demchuk, D. V., and Terent'ev, A. O.: Rearrangements of organic peroxides and

related processes, Beilstein J. Org. Chem, 12, 1647-1748, 10.3762/bjoc.12.162, 2016.

Yasmeen, F., Sauret, N., Gal, J. F., Maria, P. C., Massi, L., Maenhaut, W., and Claeys, M.: Characterization of oligomers from methylglyoxal under dark conditions: a pathway to produce secondary organic aerosol through cloud processing during nighttime, Atmospheric Chemistry and Physics, 10, 3803-3812, 10.5194/acp-10-3803-2010, 2010.

You, B., Li, S. Y., Tsona, N. T., Li, J. L., Xu, L., Yang, Z. M., Cheng, S. M., Chen, Q. C., George, C., Ge, M. F., and Du, L.: Environmental processing of short-chain fatty alcohols induced by photosensitized chemistry of brown carbons, ACS Earth Space Chem., 4, 631-640, 10.1021/acsearthspacechem.0c00023, 2020.

Zhang, J., Shrivastava, M., Zelenyuk, A., Zaveri, R. A., Surratt, J. D., Riva, M., Bell, D., and Glasius, M.: Observationally constrained modeling of the reactive uptake of isoprene-derived epoxydiols under elevated relative humidity and varying acidity of seed aerosol conditions, ACS Earth Space Chem., 7, 788-799, 10.1021/acsearthspacechem.2c00358, 2023.

Zhang, R., Wang, G., Guo, S., Zamora, M. L., Ying, Q., Lin, Y., Wang, W., Hu, M., and Wang, Y.: Formation of urban fine particulate matter, Chem. Rev., 115, 3803-3855, 10.1021/acs.chemrev.5b00067, 2015a.

Zhang, S., Li, D., Ge, S., Wu, C., Xu, X., Liu, X., Li, R., Zhang, F., and Wang, G.: Elucidating the mechanism on the transition-metal ion-synergetic-catalyzed oxidation of SO_2 with implications for sulfate formation in Beijing haze, Environmental Science & Technology, 58, 2912-2921, 10.1021/acs.est.3c08411, 2024.

Zhang, S., Li, D., Ge, S., Liu, S., Wu, C., Wang, Y., Chen, Y., Lv, S., Wang, F., Meng, J., and Wang, G.: Rapid sulfate formation from synergetic oxidation of SO_2 by O_3 and NO_2 under ammonia-rich conditions: Implications for the explosive growth of atmospheric $PM_{2.5}$ during haze events in China, Sci. Total Environ., 772, 144897, 10.1016/j.scitotenv.2020.144897, 2021.

Zhang, X., Schwantes, R. H., McVay, R. C., Lignell, H., Coggon, M. M., Flagan, R. C., and Seinfeld, J. H.: Vapor wall deposition in Teflon chambers, Atmos. Chem. Phys., 15, 4197-4214, 10.5194/acp-15-4197-2015, 2015b.

Zhang, Y. M., He, L., Sun, X. M., Ventura, O. N., and Herrmann, H.: Theoretical Investigation on the Oligomerization of Methylglyoxal and Glyoxal in Aqueous Atmospheric Aerosol Particles, Acs Earth and Space Chemistry, 6, 1031-1043, 10.1021/acsearthspacechem.1c00422, 2022.

Zhao, J., Levitt, N. P., Zhang, R., and Chen, J.: Heterogeneous Reactions of methylglyoxal in acidic media: Implications for secondary organic aerosol formation, Environmental Science & Technology, 40, 7682-7687, 10.1021/es060610k, 2006.

Zhao, R., Aljawhary, D., Lee, A. K. Y., and Abbatt, J. P. D.: Rapid aqueous-phase photooxidation of dimers in the α-pinene secondary organic aerosol, Environ. Sci. Technol. Lett., 4, 205-210, 10.1021/acs.estlett.7b00148, 2017.

Zheng, H., Chang, X., Wang, S., Li, S., Zhao, B., Dong, Z., Ding, D., Jiang, Y., Huang, G., Huang, C., An, J., Zhou, M., Qiao, L., and Xing, J.: Sources of Organic Aerosol in China from 2005 to 2019: A Modeling Analysis, Environmental Science & Technology, 57, 5957-5966, 10.1021/acs.est.2c08315, 2023.

726

727

728

729

Table 1. Concentrations of total SOA formed in the chamber and that formed only from the uptake of methylglyoxal (MGly) in the chamber

Seed	SOA[a] (μg m^{-3})	Surface area of seeds (m^2 m^{-3})	MGly (μg m^{-3})	γ[b]	SOA$_{MGly}$[c] (μg m^{-3})	SOA/SOA$_{MGly}$
Na$_2$SO$_4$	140	9.30×10^{-3}	26.74	2.6×10^{-4}	17.17	8.2
(NH$_4$)$_2$SO$_4$	101	1.95×10^{-2}	42.95	2.6×10^{-4}	28.88	3.5
NH$_4$HSO$_4$	57	1.14×10^{-2}	38.43	2.6×10^{-4}	20.17	2.8

[a]SOA values are the concentrations of SOA on different seeds observed in the experiments. [b]The values of γ are consistent with the parameters of the irreversible uptake of MGly used in CMAQ v5.3.[c]SOA$_{MGly}$ is estimated concentration of SOA formed from the irreversible uptake of MGly on different aerosols.

735

736

737

738

739

Figure Captions

Figure 1. Time evolution of gas-phase and aerosol-phase species in the presence of $(NH_4)_2SO_4$ seeds during acetone oxidation process (Phase I: Photochemical reactions of acetone by OH radicals without NH_3; Phase II: Reaction of acetone oxidation products with NH_3 under dark conditions) (a) Gas-phase compounds; (b) SOA and molar ratio of NH_4^+ to SO_4^{2-} in the aerosol-phase; (c) N/C and O/C elemental ratios and oxidation state of compounds (OSc, $2 \times O/C$-H/C) of SOA; (d) Relative abundances of CO_2^+, the sum of CHO^+ plus $C_2H_3O^+$, and CHN family fragments of SOA.

Figure 2. Fragment compositions of acetone-derived SOA in the presence of $(NH_4)_2SO_4$ seeds between the two reaction phases. (Phase I: Oxidation of acetone by OH radicals without NH_3; Phase II: Reaction of acetone oxidation products with NH_3 under dark conditions)

Figure 3. Effect of seed acidity on SOA formation. (a) The amount SOA normalized by the surface area (SA) of aerosols and OSc of SOA in the presence of different seeds at Phase I; (b) Effective Henry's law constants ($K_{H, salt}$) of MGly and acidity (pH) of inorganic aerosols during the reaction; (c) and (d) Mass spectra of SOA from acetone oxidations by OH radicals with no NH_3 in the presence of Na_2SO_4 and $(NH_4)_2SO_4$ seeds, respectively.

Figure 4. Effect of ammonia on SOA formation. (a) The Difference in N/C ratio of Phase II relative to Phase I on different seeds; (b) Partitioning coefficients of NH_3 ($\varepsilon(NH_4^+)$) on different seeds in the chamber; (c) MAC of acetone-derived SOA in the presence of different seeds; (d) Mass spectrum of 1H-imidazole-4-carboxylic acid formed during the heterogeneous oxidation of acetone in the presence of $(NH_4)_2SO_4$ seed.
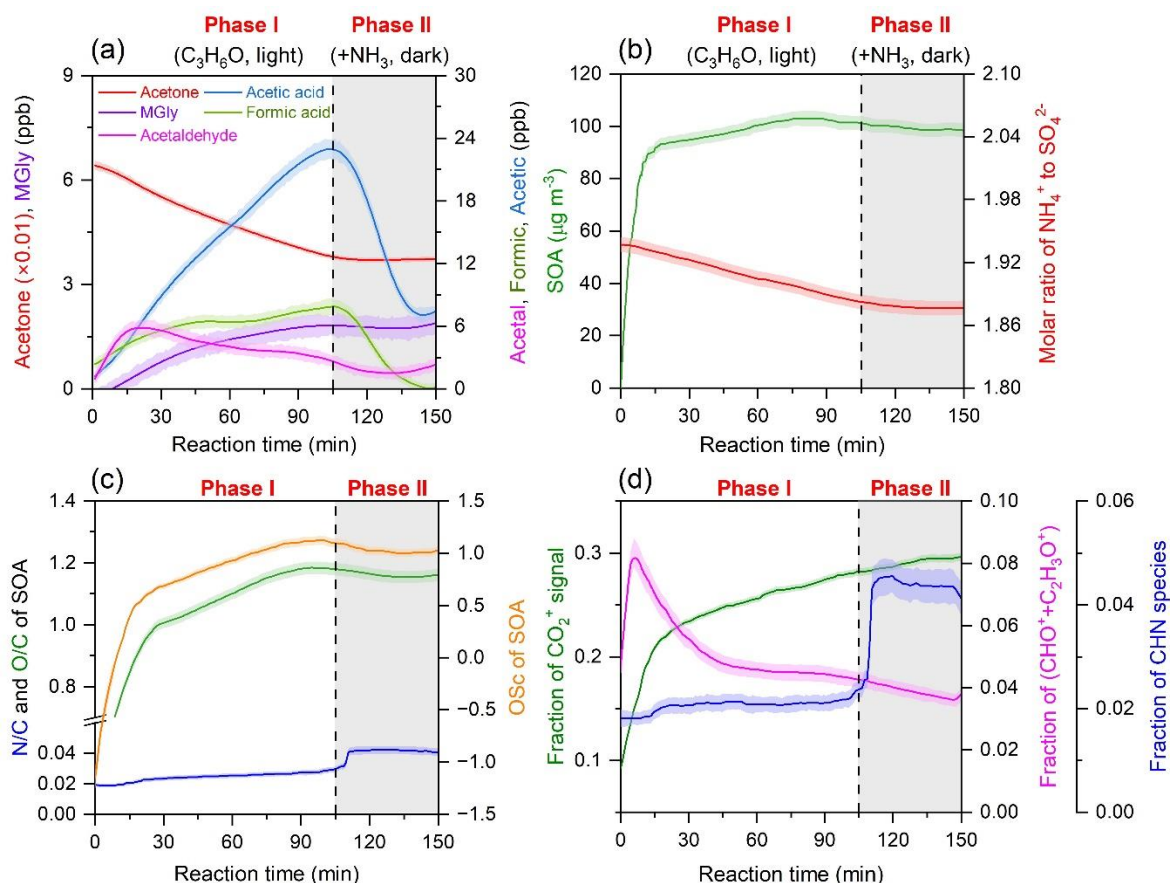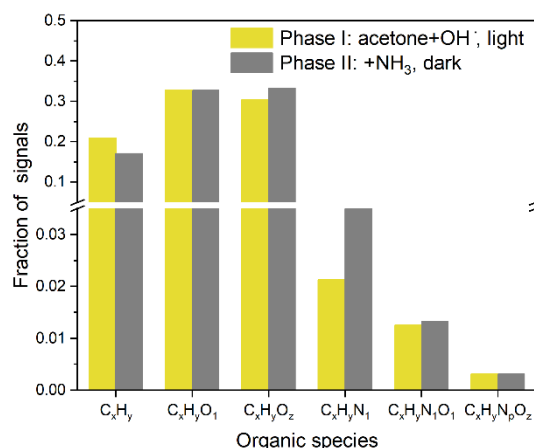
Figure 5. SOA yield (green) and $MAC_{\lambda=270 \text{ nm}}$ (red) of acetone-derived SOA in the presence of Na_2SO_4 and $(NH_4)_2SO_4$ seeds with NH_3 under dark conditions (Phase II), respectively.

Figure 6. A diagram for the formation pathway of SOA derived from acetone oxidation in the atmosphere.

Figure 1. Time evolution of gas-phase and aerosol-phase species in the presence of $(NH_4)_2SO_4$ seeds during acetone oxidation process (Phase I: Photochemical reactions of acetone by OH radicals without NH_3; Phase II: Reaction of acetone oxidation products with NH_3 under dark conditions) (a) Gas-phase compounds; (b) SOA and molar ratio of NH_4^+ to SO_4^{2-} in the aerosol-phase; (c) N/C and O/C elemental ratios and oxidation state of compounds (OSc, 2×O/C-H/C) of SOA; (d) Relative abundances of CO_2^+, the sum of CHO^+ plus $C_2H_3O^+$, and CHN family fragments of SOA.

Figure 2. Fragment compositions of acetone-derived SOA in the presence of $(NH_4)_2SO_4$ seeds between the two reaction phases. (Phase I: Oxidation of acetone by OH radicals without NH_3; Phase II: Reaction of acetone oxidation products with NH_3 under dark conditions)

Figure 3. Effect of seed acidity on SOA formation. (a) The amount SOA normalized by the surface area (SA) of aerosols and OSc of SOA in the presence of different seeds at Phase I; (b) Effective Henry's law constants ($K_{H, salt}$) of MGly and acidity (pH) of inorganic aerosols during the reaction; (c) and (d) Mass spectra of SOA from acetone oxidations by OH radicals with no NH_3 in the presence of Na_2SO_4 and $(NH_4)_2SO_4$ seeds, respectively.

28

806

807 **Figure 4**. Effect of ammonia on SOA formation. (a) The Difference in N/C ratio of Phase II

808 relative to Phase I on different seeds; (b) Partitioning coefficients of NH_3 ($\varepsilon(NH_4^+)$) on

809 different seeds in the chamber; (c) MAC of acetone-derived SOA in the presence of different

810 seeds; (d) Mass spectrum of 1H-imidazole-4-carboxylic acid formed during the

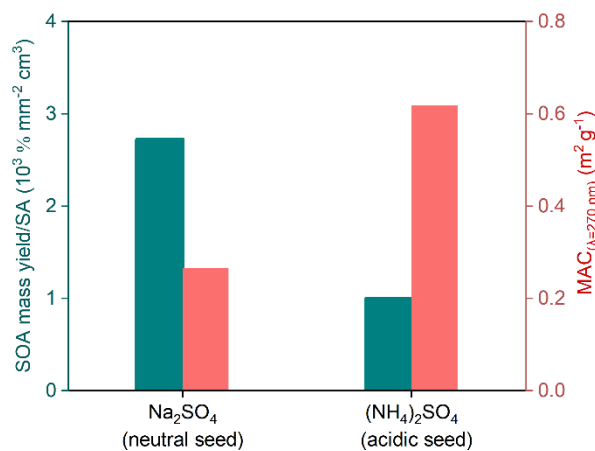811 heterogeneous oxidation of acetone in the presence of $(NH_4)_2SO_4$ seed.
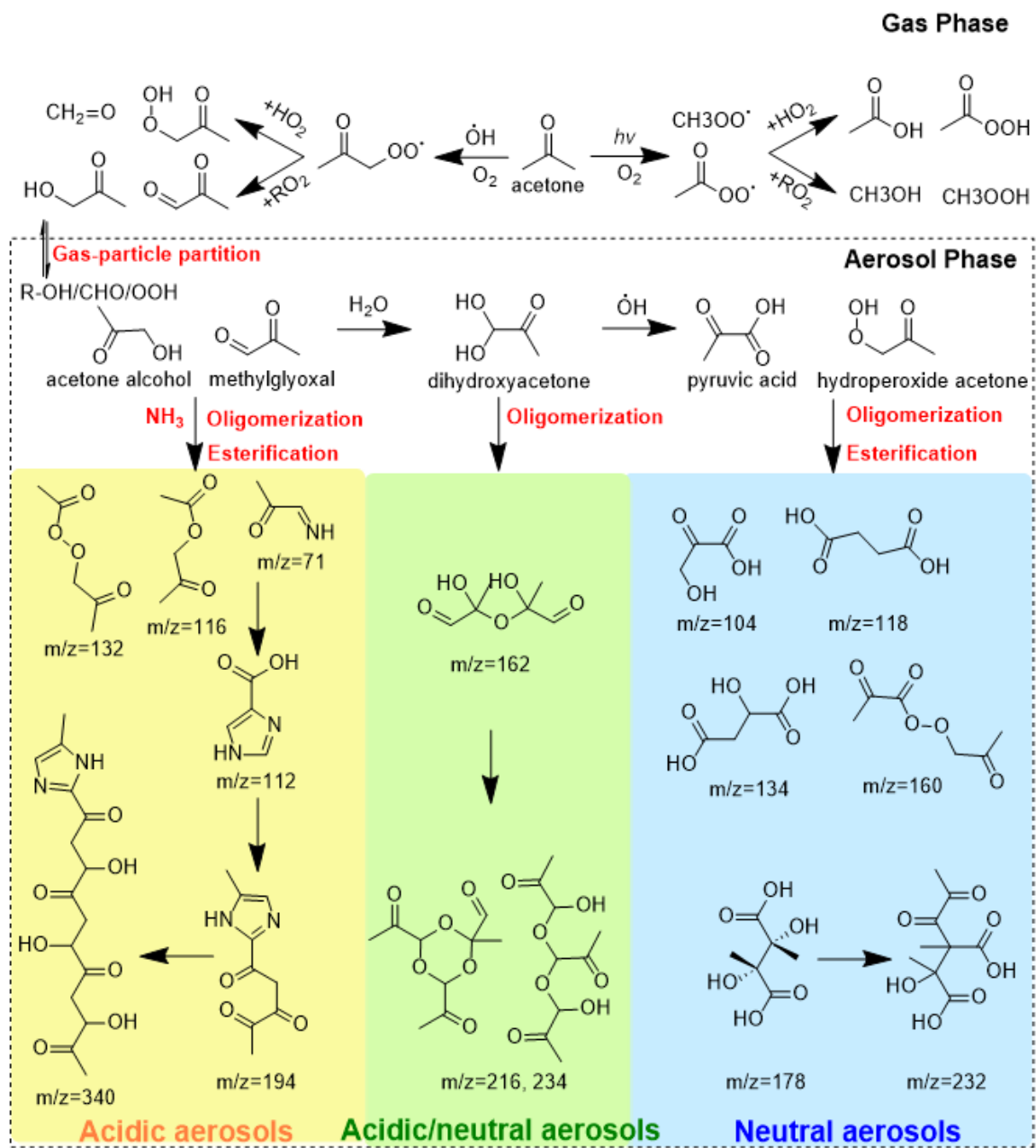
812

813

814

815

816

817

818 **Figure 5**. SOA yield (green) and $MAC_{\lambda=270\ nm}$ (red) of acetone-derived SOA in the presence

819 of Na_2SO_4 and $(NH_4)_2SO_4$ seeds with NH_3 under dark conditions (Phase II), respectively.

820

821

Figure 6. A diagram for the formation pathway of SOA derived from acetone oxidation in the atmosphere.

824